

The Neutrophil Lipocalin NGAL Is a Bacteriostatic Agent that Interferes with Siderophore-Mediated Iron Acquisition

David H. Goetz,^{1,2} Margaret A. Holmes,²
Niels Borregaard,³ Martin E. Bluhm,⁴
Kenneth N. Raymond,⁴ and Roland K. Strong^{2,5}

¹Molecular and Cellular Biology Program
Fred Hutchinson Cancer Research Center
Box 357275

University of Washington
Seattle, Washington 98105

²Division of Basic Sciences
Fred Hutchinson Cancer Research Center
1100 Fairview Avenue North
Seattle, Washington 98109

³The Granulocyte Research Laboratory
Department of Hematology
Rigshospitalet
Copenhagen
Denmark

⁴Department of Chemistry
University of California
Berkeley, California 94720

Summary

First identified as a neutrophil granule component, neutrophil gelatinase-associated lipocalin (NGAL; also called human neutrophil lipocalin, 24p3, uterocalin, or *neu*-related lipocalin) is a member of the lipocalin family of binding proteins. Putative NGAL ligands, including neutrophil chemotactic agents such as N-formylated tripeptides, have all been refuted by recent biochemical and structural results. NGAL has subsequently been implicated in diverse cellular processes, but without a characterized ligand, the molecular basis of these functions remained mysterious. Here we report that NGAL tightly binds bacterial catecholate-type ferric siderophores through a cyclically permuted, hybrid electrostatic/cation- π interaction and is a potent bacteriostatic agent in iron-limiting conditions. We therefore propose that NGAL participates in the antibacterial iron depletion strategy of the innate immune system.

Introduction

Lipocalins are a functionally diverse family of proteins that generally bind small, hydrophobic ligands (Åkerstrom et al., 2000a) and interact with cell-surface receptors (Flower, 2000). The family is defined by a highly conserved fold, despite limited sequence conservation. The core structure consists of an eight-stranded antiparallel β barrel that defines the calyx, or cup-shaped ligand binding site, and accessory elements (Flower et al., 2000). Lipocalins generally act as transporters (though some are enzymes), trafficking small molecules to specific cells, and are thus proposed to be variously involved in retinol transport, invertebrate cryptic color-

ation, olfaction, pheromone transport, prostaglandin synthesis, modulation of cell growth and metabolism, regulation of the immune response, tissue development, and animal behavior. However, some of these functional assignments have been made on very indirect or circumstantial evidence, without determination of the actual molecular mechanisms involved. The importance of the lipocalin family is reflected in the recent dedication of an entire volume of *Biochimica et Biophysica Acta* (Åkerstrom et al., 2000b) to a review of these proteins.

Human neutrophil gelatinase-associated lipocalin (NGAL; also called human neutrophil lipocalin) was originally identified as a component of neutrophil granules but is also expressed in epithelial cells in response to inflammatory signals (Kjeldsen et al., 2000). The rat ortholog, *neu*-related lipocalin (NRL) or α_2 -microglobulin-related protein, was identified as a protein highly overexpressed in mammary cancers. The murine ortholog, called 24p3, 24 kDa superinducible protein (Sip24), or uterocalin, was identified as a protein induced in response to various proliferative signals and is highly expressed in uterine luminal fluids and epithelial cells. Recently, 24p3 has also been implicated in processes as diverse as apoptosis (Devireddy et al., 2001) and kidney cell differentiation (Yang et al., 2002 [this issue of *Molecular Cell*]). NGAL, like most lipocalins, is thought to modulate cellular processes by binding to ligand(s) and interacting with specific cell-surface receptors. Evidence for such a mammalian receptor for NGAL has recently been reported (Devireddy et al., 2001). One early hypothesis proposed that NGAL has immunomodulatory activity by binding and clearing lipophilic inflammatory mediators (Bundgaard et al., 1994), such as the neutrophil tripeptide chemoattractant N-formyl-Met-Leu-Phe (Chu et al., 1997; Sengelov et al., 1994).

Structures of NGAL determined by X-ray crystallography (Goetz et al., 2000) and nuclear magnetic resonance spectroscopy (Coles et al., 1999) reveal that the calyx of NGAL is shallower and broader than is typical of most lipocalins and is also uncharacteristically lined with polar and positively charged residues. The incompatible nature of the NGAL calyx, together with binding data showing millimolar dissociation constants (Bratt et al., 1999), demonstrates that NGAL does not specifically bind N-formylated tripeptides or other hydrophobic ligands. In this report, we alternatively show that NGAL binds a negatively charged ferric siderophore with a subnanomolar dissociation constant and acts as a potent bacteriostatic agent by sequestering iron. While crystallography has previously been used to determine the identity of an unknown protein ligand (for instance, the furanosyl borate diester bound by the bacterial quorum sensor protein LuxP; Chen et al., 2002) or to make dramatic leaps in understanding protein function through characterizing ligand interactions (antigenic peptide presentation by MHC class I proteins; Bjorkman et al., 1987), this study represents one of the rare examples of determining the function of a previously mysterious protein by relying primarily on crystallography to identify its ligand.

⁵ Correspondence: rstrong@fhcrc.org

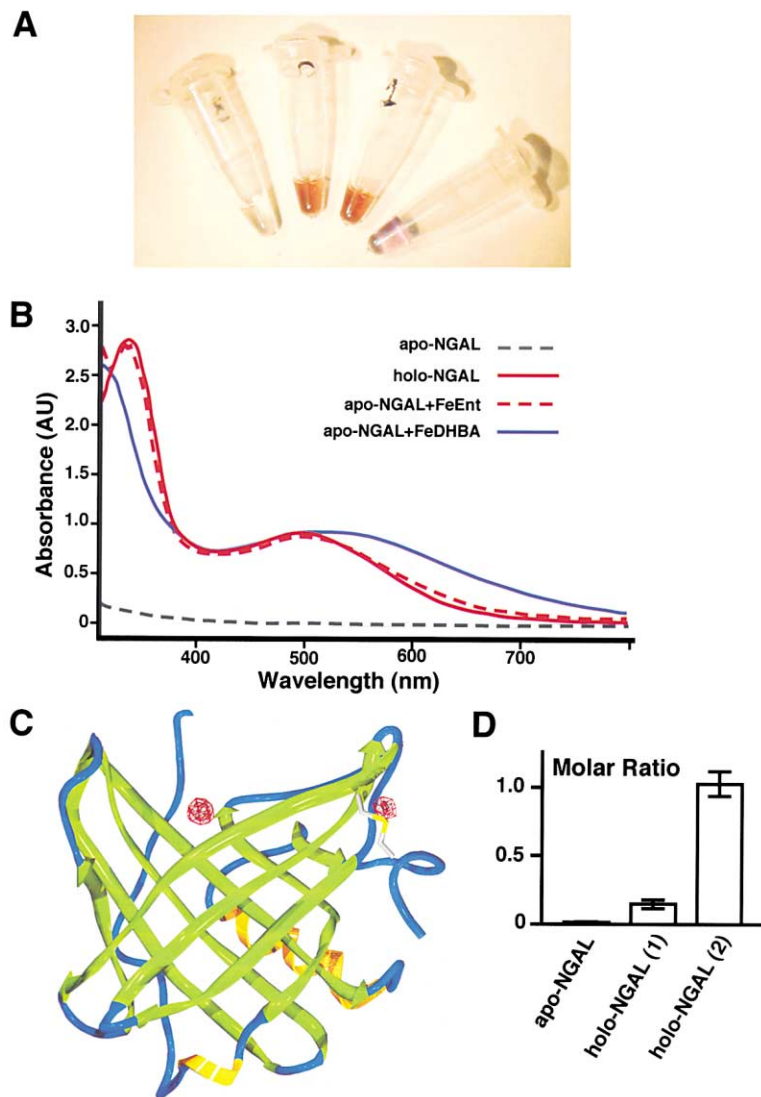


Figure 1. NGAL Copurifies with a Bacterial Chromophore

(A) Tubes of purified NGAL (at between 10 and 15 mg/ml) are shown, from left to right: from *E. coli* BL21 (apo-NGAL), from XL1-Blue (holo-NGAL), apo-NGAL saturated with FeEnt, and apo-NGAL saturated with FeDHBA.

(B) Spectra of various forms of NGAL, all at approximately 170 μ M, are displayed.

(C) The 3.4 Å native anomalous difference electron density map is shown contoured at 3.0σ (red) and 5.5σ (dark red) superimposed on a ribbon representation of the NGAL structure and colored by secondary structure (helices, yellow; strands, green; coil, blue).

(D) The iron:protein molar ratio, determined by AA, is plotted. Iron:apo-NGAL is approximately 0.005; iron:holo-NGAL (1), expressed in minimal media plus 10 μ M iron, is 0.17; and iron:holo-NGAL (2), expressed in rich media, is essentially unity.

Results and Discussion

NGAL Tightly and Specifically Binds a Bacterial Chromophore

Human NGAL copurifies with an intensely red colored chromophore (holo-NGAL; Figures 1A and 1B) when expressed heterologously in the XL1-Blue strain of *E. coli* (Stratagene) as a fusion protein with glutathione-S-transferase (Bundgaard et al., 1994). The holo-NGAL complex is stable over a pH range from below 3 to above 7.5 or in 8 M urea plus 2% w/w SDS for over 24 hr at ambient temperature (data not shown). The chromophore can be separated from the protein by polyacrylamide gel electrophoresis (PAGE) after boiling in 8 M urea (data not shown). The chromophore migrates at the dye front in these gels, indicating a large negative charge-to-mass ratio.

We crystallized monomeric, bacterially expressed holo-NGAL at neutral pH using conditions initially determined for monomeric, baculovirus-expressed NGAL (Goetz et al., 2000). A preliminary 3.4 Å resolution diffraction data set was collected with Cu-K α radiation. The

previously described crystal form contained two ordered monomers in the asymmetric unit; here, however, a crystal dehydration step prior to data collection resulted in three ordered molecules in the asymmetric unit (referred to as molecules A, B, and C) and a 1% reduction along the c-edge of the unit cell. Density was present in the original baculovirus NGAL structure that could not be fit with an additional protein monomer in the region where we now find a third molecule. We presume that the initial structure included a third molecule that was either incompletely occupied or partially disordered or both and that the current crystal treatment, and/or the absence of N-linked oligosaccharide on the bacterially expressed NGAL resolved these shortcomings. The resultant medium-resolution $F_{\text{obs}}-F_{\text{calc}}$ difference electron density map revealed a large blob of positive electron density, not accounted for by protein atoms, in the calyx, centered between the guanidinium group of Arg81 and the N_{ϵ} atoms of Lys125 and Lys134. The location of this feature, centered in the NGAL calyx, strongly suggested that the chromophore was indeed a specific ligand of NGAL, and its proximity to positively charged residues

was consistent with the overall negative charge shown by PAGE. A native anomalous difference electron density map further revealed two significant peaks: one, with a height of 5.7σ , corresponding to the single disulfide bond in NGAL; the other, with a height of 7.2σ , centered in the blob of $F_{\text{obs}} - F_{\text{calc}}$ difference density (Figure 1C). The height, size, and shape of the anomalous peak suggested that the chromophore contained a single heavy atom.

The Bacterial Chromophore Contains an Iron Atom

The identity of the heavy atom as iron, strongly suggested by the red color of the chromophore, was confirmed by atomic absorption (AA) and X-ray fluorescence spectroscopy (at beamline 5.0.2 at the Advanced Light Source [ALS], Berkeley, CA). The molar ratio of iron to protein determined by AA was variable among different protein preparations yet never exceeded 1:1 (Figure 1D). This ratio was consistent with the anomalous difference density feature and confirmed that each molecule of NGAL has the capacity to bind a single iron atom-containing bacterial chromophore in its calyx. In addition, nearly colorless protein, with less than 1% iron-containing chromophore by AA (apo-NGAL), can be prepared using the BL21 strain of *E. coli* (Figures 1A, 1B, and 1D).

Iron is required by all aerobic organisms (Neilands, 1995). Within the body, the majority of iron is bound up in hemoglobin, though several proteins bind iron directly. Transferrin transports iron between cells and is normally 30%–40% iron-saturated in the serum (Ponka et al., 1998). Iron is stored intracellularly in complex with ferritins (Harrison and Arosio, 1996). Lactoferrin is a potent bacteriostatic agent, first discovered in milk, that is released from neutrophil granules at sites of inflammation, directly inhibiting growth by sequestering iron (Ellison, 1994). It has long been thought that the body lowers available iron in response to both infection and cancer in order to slow or stop the growth of pathogens and tumors (Weinberg, 1984). The observation that giving iron supplements to patients with bacterial infection worsens their condition (Weinberg, 1984) demonstrates the scarcity of free iron in the body, with a serum concentration estimated to be as low as 10^{-24} M (Otto et al., 1992), and the efficiency of iron sequestration as an antibiotic.

NGAL Binds Iron Only in Complex with a Nonheme Compound

The large size and positive charge of the NGAL calyx, and the size of the $F_{\text{obs}} - F_{\text{calc}}$ electron density feature in the calyx, suggested that NGAL, unlike lactoferrin or transferrin, could not bind positively charged iron ions directly, a supposition we confirmed by iron binding experiments with apo-NGAL (data not shown). Nitrophorin, an insect lipocalin, binds heme (Weichsel et al., 1998) and is closely related to NGAL structurally (Goetz et al., 2000), raising the question of whether the holo-NGAL ligand could be heme or a derivative. Nitrophorin has a coin-slot shaped calyx with a slightly negative surface potential complementary to planar heme molecules. Therefore, the incompatible shape and character of the NGAL calyx, and the shape of the difference electron

density feature, rule out heme as a candidate ligand for NGAL.

When iron is limiting, many microorganisms obtain iron from the environment through the synthesis, secretion, and reuptake of small-molecule iron chelators called siderophores (Braun and Killmann, 1999). Many bacterial siderophores bind iron orders of magnitude more tightly than lactoferrin or transferrin, directly out-competing these mammalian proteins for iron during infection (Ratledge and Dover, 2000). Siderophores generally fall into two chemical classes: catecholates and hydroxamates (Neilands, 1981). The primary siderophores of *E. coli* and related enteric bacteria are the catecholate-type siderophore enterobactin (Ent; Figure 2A) (Pollack and Neilands, 1970) and the citrate-based, hydroxamate-type siderophore aerobactin (Gibson and Magrath, 1969). Ent exhibits the highest affinity for iron(III) of any known molecule, with a K_d of 10^{-49} M (Loomis and Raymond, 1991). Aerobactin expression is a key determinant of virulence for invasive strains of *E. coli* (Wooldridge and Williams, 1993).

The Holo-NGAL Ligand Is Ferric Enterobactin

To determine whether the copurified chromophore might be a ferric siderophore, apo-NGAL was mixed with ferric aerobactin or ferric Ent (FeEnt), washed extensively by dialysis or ultrafiltration, and assayed for binding by AA and spectroscopy. No detectable aerobactin binding was observed, consistent with the inability of laboratory strains of *E. coli* to synthesize aerobactin. On the other hand, FeEnt readily formed complexes with apo-NGAL that were identical to holo-NGAL both visually and spectroscopically (Figures 1A and 1B). Tryptophan fluorescence quenching analysis of the NGAL:FeEnt interaction yielded a K_d of 0.41 ± 0.11 nM at 20°C (Figure 2B), an extremely strong affinity unlikely due to serendipity. Subsequent qualitative binding assays confirm that NGAL does not bind any hydroxamate-type ferric siderophores tested (rhodotorulic acid, desferrioxamine B, or ferrichrome [Sigma]) with any appreciable affinity, but does bind other catecholate-type ferric siderophores tightly (parabactin and cepabactin).

In order to more directly characterize the holo-NGAL ligand, we refined the structure against higher resolution (2.4 Å) diffraction data subsequently collected at the ALS. The three protein molecules in the holo-NGAL structure display the classic lipocalin fold (Figure 1C) and are essentially identical to each other and the three molecules in the two crystal forms of NGAL previously described (Goetz et al., 2000), with pair-wise root mean square deviations (rmsd) of 0.76 \AA or less on all common C α s. The lack of differences between all three crystal structures, a total of six different views of the molecule, suggests that NGAL is quite rigid, stable, and does not undergo notable conformational changes due to crystal packing, ligand binding, ionic strength (from zero to saturating ammonium sulfate), or pH (from 4.5 to 7.0).

FeEnt Is Partially Degraded in the Holo-NGAL Crystals

In solution, FeEnt rapidly breaks down within days into dihydroxybenzoyl-serine (DHBS) and dihydroxybenzoic acid (DHBA) (O'Brien and Gibson, 1970). However, complexed with NGAL, FeEnt is stable for up to 1 month,

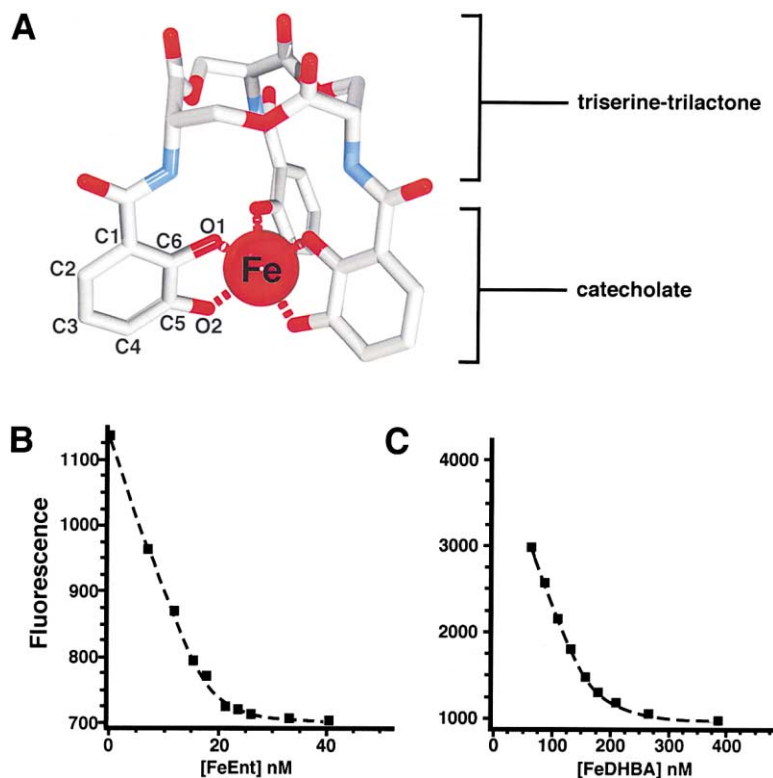


Figure 2. NGAL Binds FeEnt and FeDHBA
(A) The structure of FeEnt color-coded by atom type (carbon, gray; nitrogen, blue; oxygen, red; iron, red sphere) is displayed with the catecholate atoms and the iron labeled. (B and C) The intrinsic tryptophan fluorescence quenching analyses of the NGAL:FeEnt (B) and NGAL:FeDHBA (C) interactions are plotted as total fluorescence versus ligand concentration. The dashed line indicates the best-fit line for a one-site binding model calculated by nonlinear regression.

as assayed spectroscopically (data not shown). Despite this, it was apparent after several rounds of model building and refinement that the triserine-trilactone backbone of the ligand in the holo-NGAL structure was at least partially degraded, based both on difference electron density maps (Figure 3A) and unusually high FeEnt libration tensors following TLS refinement. Ligand degradation is not inconsistent with the protective effect of NGAL on Ent, considering that diffraction-quality crystals required fully 7 months to grow. Parallel refinements were therefore performed, modeling the ligand density as either FeEnt or as a mixed complex of ferric DHBS and DHBA (which we term FeDHBx). To validate that FeDHBA is a ligand, we also measured the affinity of the NGAL:FeDHBA interaction by tryptophan fluorescence quenching ($K_d = 7.9 \pm 1.8$ nM; Figure 2C). Though weaker than the affinity for FeEnt, the value is still respectable and demonstrates that FeDHBA is a NGAL ligand. Even though reasonable R_{work} and R_{free} values of 23.8% and 28.0% were reached with intact FeEnt as the ligand, it is clear that the ligand density is better modeled as FeDHBx (Figures 3B and 3C), yielding R_{work} and R_{free} values that are 1.3% and 0.9% better, respectively. The final statistics reported in Table 1 and the coordinates deposited in the Protein Data Bank (PDB; accession code 1L6M) (Berman et al., 2000) therefore reflect the final NGAL:FeDHBx complex structure. However, we feel that the NGAL:FeEnt complex structure is a valid model of the NGAL:FeEnt interaction, described below, because we can refine a reasonable structure with FeEnt as the ligand, because NGAL primarily interacts with structural elements common to both FeEnt and FeDHBx, and because, in reality, the holo-NGAL

ligand in the crystal is probably best described as a mixture of intact and partially degraded FeEnt. In either refinement, the density clearly shows the siderophore binding iron in a phenolate mode, with all six catecholate hydroxyls contributing iron bonds, and therefore deprotonated, rather than displaying salicylate-mode binding, where the three O2 hydroxyls are protonated and the three iron ligands thus lost are replaced by the amide carbonyls at the DHBA/serine linkages.

NGAL and FeEnt Interact Predominately through Charge Complementarity and Cyclically Permuted Cation- π Interactions

NGAL binds FeEnt by intercalating the positively charged side chains of three protein residues (Arg81, Lys125, and Lys134) between the ligand catecholates, each of which sits in a distinct subpocket of the trilobate calyx (Figures 4A and 4B). Ent is uncharged, but FeEnt carries a net charge of -3 (Raymond et al., 1984) highly delocalized over the molecule, as shown by semi-empirical calculations (Figure 4C). Therefore, the NGAL:FeEnt interaction clearly has an electrostatic component. However, the positively charged groups of the intercalating side chains are also in position to make favorable protein:cation- π interactions (Gallivan and Dougherty, 1999) with the ligand (Figure 4D). Cation- π interactions in proteins occur between the positive charge of a lysine or arginine side chain and the quadrupole moment associated with the delocalized π -electrons of an aromatic functional group such as a tryptophan, tyrosine, or phenylalanine (Dougherty, 1996). An example is the binding of phosphotyrosine-containing peptides to SH2 domains (Yaffe, 2002), where a pair of

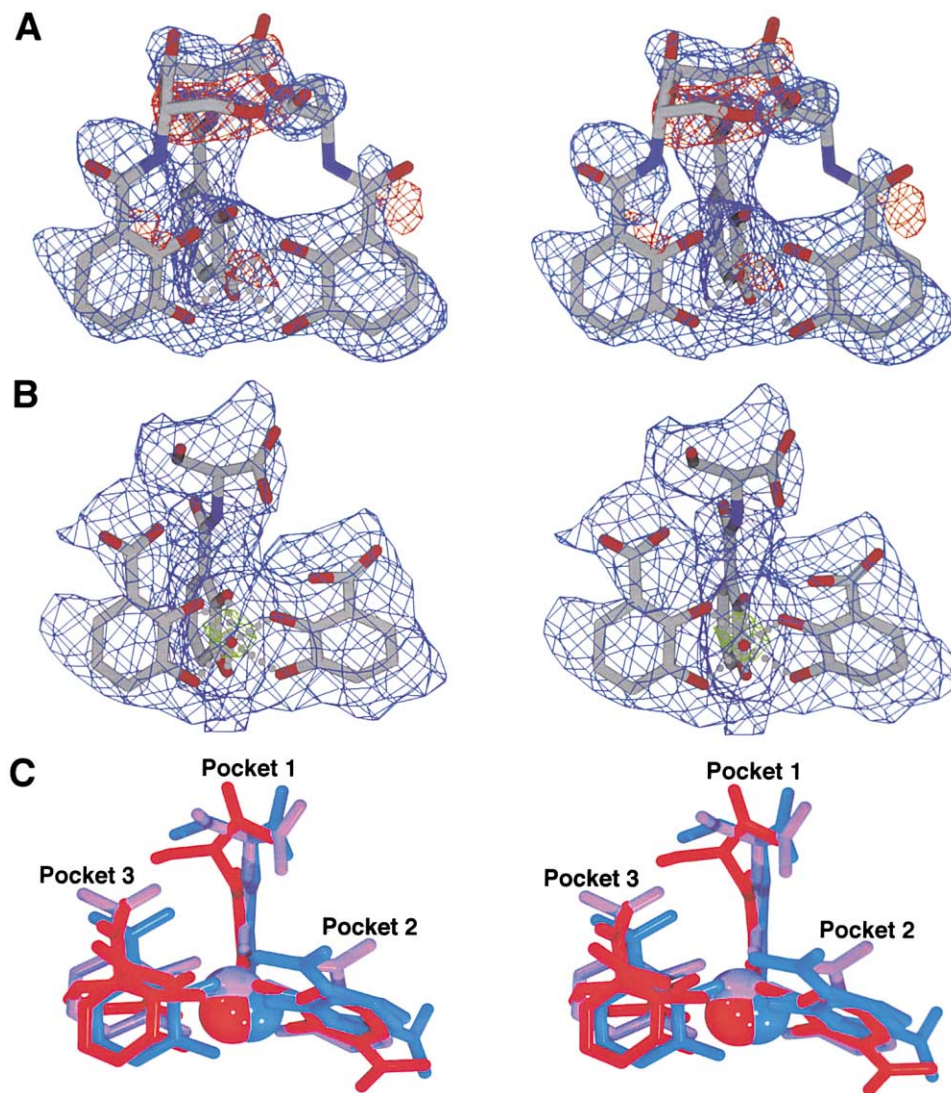


Figure 3. Ligand Electron Density Maps

(A and B) Stereoviews are displayed of the alternatively refined final electron density maps superimposed on the structures of (A) FeEnt (blue, $2F_{\text{obs}}-F_{\text{calc}}$, contoured at 1σ ; red, $F_{\text{obs}}-F_{\text{calc}}$, contoured at -3σ) and (B) FeDHBx (blue, omit-refined $2F_{\text{obs}}-F_{\text{calc}}$, contoured at 1σ ; green, omit-refined $2F_{\text{obs}}-F_{\text{calc}}$, contoured at 3σ). No significant negative density features are present in the region of the ligand in the FeDHBx model. The electron density is inconsistent with a salicylate-type interaction between FeEnt and iron, in part because the catechol rings would be more splayed-out in salicylate-mode binding.

(C) A stereoview of a superposition of the three FeDHBx molecules in the asymmetric unit (molecule A, blue; B, purple; C, red) is shown with the iron atoms represented as spheres. All views in this figure place the DHBS bound in pocket 1 at the back.

positively charged side chains (lysine and/or arginine) interact with the phosphotyrosine side chain. However, the negative charge of the phosphate moiety is not delocalized over the tyrosine aromatic group. Therefore the NGAL:FeEnt interaction is a novel hybrid between simple ionic and cation- π interactions, one where the interacting groups are interlaced, cation-catecholate-cation-catecholate, in a cyclically permuted manner around the iron atom.

Additional stabilizing van der Waals and hydrogen bonds are made by residues lining the three pockets in the calyx (Figures 4E and 4F). However, these interactions are not all uniformly present across the three calyces in the structure, and the overall impression of the

NGAL:FeEnt interaction is that the ligand is fairly loosely held in the calyx, with the high affinity due primarily to the hybrid electrostatic/cation- π bonds. In pocket 1, the catecholate lies sandwiched between the side chains of Lys134 and Lys125. The floor and wall of this pocket are formed by Phe123, Tyr132, Phe133, and the loop formed by residues 38 through 41. Tyr106 hydrogen bonds to the O2 atom of the catecholate. The only contacts to the triserine-trilactone backbone of FeEnt are made in this pocket: van der Waals contacts from Ala40 and water-mediated hydrogen bonds between the carbonyl oxygen of the amide connecting the catecholate to the backbone of Ent and the peptide amines of Asn39 and Ala40 and the side chain carbonyl of Asn39. Less

Table 1. Crystallographic Statistics

Data collection and processing	
Resolution (Å)	20–2.40 (2.44–2.40)
Observations	312,664
Unique reflections	30,746
Completeness (%)	100 (100)
I/σ(I)	37.3 (3.8)
R _{sym} (%)	5.7 (51)
Cell dimensions (Å)	a = b = 115.1; c = 115.2 (P4 ₁ ,2 ₁ ,2)
Refinement	
Resolution (Å)	19.76–2.40 (2.46–2.40)
Reflections (all F > 0)	28,156
Protein atoms (3 molecules/a. u.)	4,222
Ligand atoms	143
Solvent atoms	111 (2 SO ₄ ²⁻ , 7 glycerol)
R _{work} (%)	22.5 (25.0)
R _{free} (%) (on 1,470 reflections)	27.1 (35.9)
Rmsd from ideality: bonds (Å)	0.013
Rmsd from ideality: bond angles (°)	2.0
Average B factor (Å ²)	37.1
Ramachandran plot	
Most favored (%)	86.6
Additional allowed (%)	11.6
Generously allowed (%)	1.8
Disallowed (%)	0

Numbers in parentheses indicate values for the highest resolution shell.

extensive contacts are seen in the other pockets. The catecholate in pocket 2 sits between Lys134 and Arg81, with the pocket defined by the side chains of Tyr52, Ser68, and Trp79. Tyr106 can also hydrogen bond to the O2 atom of the pocket 2 catecholate. The Ent catecholate in pocket 3, the least well-defined and most solvent-accessible pocket, lies between Lys125 and Arg81 and is defined by the side chains of Tyr100 and Trp79. With the exception of Trp79 and Arg81, the residues that interact with FeEnt are in essentially equivalent positions in all three molecules in the asymmetric unit. Trp79 is positioned equivalently in molecules A and C, but is disordered and modeled as an alanine in molecule B. Trp79 was also alternately ordered or disordered in the original baculovirus-expressed NGAL crystal structures (Goetz et al., 2000), but when ordered was flipped almost 180° around χ_2 from where it packs against the FeEnt catecholates in pockets 2 and 3. The side chain of Arg81 adopts two different conformations: in molecules A and C, the side chain of Arg81 forms a hydrogen bond to the side chain hydroxyl of Ser68 and helps define the floor of pocket 2; in molecule B, there is a 150° rotation around the χ_1 torsion angle, orienting the side chain to occupy the space vacated by the disordered side chain of Trp79.

The sequence identity between human NGAL and murine 24p3 or rat NRL is 62.0% or 63.5%, respectively. All but 5 of the 36 residues that have an atom within 7.5 Å of a ligand atom in the NGAL:FeEnt complex structure are conserved or strongly similar. Among the five less conserved substitutions, only a phenylalanine for glutamine substitution at position 49 might come close enough to the ligand to contact, though not close enough to be expected to preclude or even significantly affect, binding. Therefore, we conclude that 24p3 and NRL are likely to have binding specificities similar to NGAL.

Only 62%–70% of the solvent-accessible surface area of FeEnt is buried by association with NGAL. The range is mostly due to whether the side chain of Trp79 makes contact with the ligand or not. In contrast, nitrophorin buries almost 90% of the solvent-accessible area of heme, even though heme is much larger than FeEnt. In addition to the relative exposure of the ligand, there are significant unfilled volumes underlying the ligand, particularly in pocket 2 (Figure 4E). This latter site had been suggested to be a carboxylic binding pocket in the initial crystallographic analysis (Goetz et al., 2000). Together, these two aspects of the complex leave considerable space around the ligand, room that could accommodate significant chemical elaboration of the basic catecholate siderophore structure. Therefore, while seemingly specific for catecholate siderophores, the NGAL calyx could likely accommodate a range of compounds.

Structures are available for several siderophore binding proteins, including the periplasmic hydroxamate-type siderophore binding protein FhuD (Clarke et al. 2002) and the cork domain outer-membrane siderophore receptors for FeEnt, FepA (Buchanan et al., 1999), ferric ferrichrome, FhuA (Ferguson et al., 1998), and ferric citrate, FecA (Ferguson et al., 2002). In the crystal structure of the FepA:FeEnt complex, both the protein binding pocket and the ligand are disordered. Thus, the structure fails to reveal the details of the FepA:FeEnt recognition mechanism, but both the crystal structure and biochemical data (Cao et al., 2000) implicate a number of positively charged and aromatic residues in the binding of FeEnt. Therefore, it may turn out that NGAL and FepA share similarities in the way in which they recognize FeEnt. However, the FhuA, FecA, and FhuD binding sites show essentially no recognizable structural similarity to the NGAL calyx, consistent with the structural dissimilarity of their respective ligands.

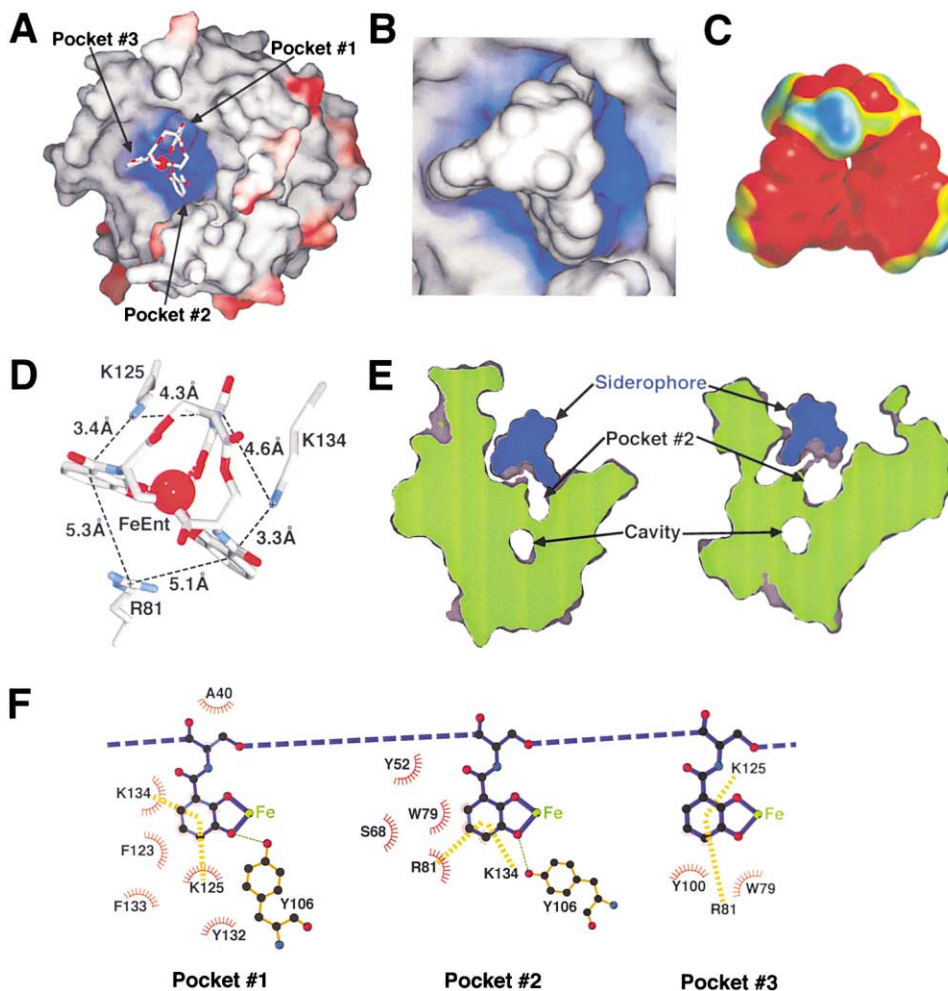


Figure 4. The NGAL:FeEnt Interaction

(A) A view of the NGAL:FeEnt complex is shown, with electrostatic potential mapped onto the molecular surface of NGAL (blue, positive; red, negative) and the ligand displayed and colored as in Figure 2A. The catechol pockets are indicated.

(B) A closeup of the calyx is shown, now with the molecular surface of FeEnt displayed (gray).

(C) The electrostatic potential of FeEnt is shown, calculated in SPARTAN using semiempirical methods (PM3D) and mapped onto the van der Waals surface of FeEnt (red, most negative; blue, least negative). The orientation of FeEnt is perpendicular to that in (A) and (B).

(D) A closeup of the cyclically permuted, hybrid electrostatic/cation- π interaction is shown, with FeEnt displayed as in Figure 2A (in the same orientation as in [A] and [B]) and the side chains of residues Arg81, Lys125, and Lys134 colored by atom type. Distances are shown from the atom indicated (+) to the center of the corresponding FeEnt catechol ring.

(E) 3 Å thick, orthogonal sections through the structure, centered on the ligand, are shown (green, NGAL; blue, FeEnt). The cavity indicated was identified in the original crystallographic analysis of NGAL (Goetz et al., 2000).

(F) The protein/ligand contacts are schematized, based upon an analysis using LIGPLOT (Wallace et al., 1995). FeEnt has been exploded to separate the three catechol pockets. Ligand bonds are colored blue; protein bonds are colored yellow; atoms are colored carbon, black; oxygen, red; nitrogen, blue; and iron, green. Hydrogen bonds are displayed as thin, dotted green lines; van der Waals interactions as red stellations; and cation- π interactions as thick, dotted yellow lines.

Differences between the NGAL:FeEnt and NGAL:FeDHBx Complex Structures

Ent is replaced with DHBS in pocket 1 and DHBA in pockets 2 and 3 in the NGAL:FeDHBx complex model (Figure 3). The serine moiety of DHBS is likely stabilized by the backbone contacts made in pocket 1, allowing its visualization in this position, when present, in electron density maps. Most of the DHBx catecholates are within 20° of their counterparts in the FeEnt complex structure, but the density is best fit by modeling multiple DHBA conformations in one pocket in each of two of the molecules in the asymmetric unit. In pocket 2 of molecule A,

two alternate conformations were modeled, with the catechol rings flipped either 42° or 160° around the C2 to C5 vector relative to the Ent catechol in this pocket (Figure 3C). The second conformation orients the carboxyl group of DHBA down into the calyx, within 1.3 Å of the previously identified carboxylate binding pocket. In pocket 3 of molecule C, one conformation essentially superimposes on the corresponding Ent catechol, but the second conformation is positioned with the DHBA ring rotated by 62° about the C2 to C6 vector relative to the first (Figure 3C). The multiple conformations and orientations of the ligand in the

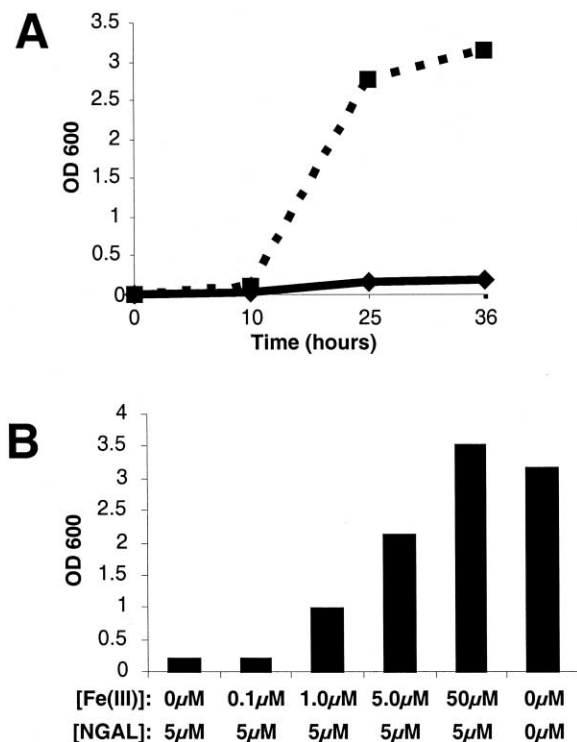


Figure 5. The Bacteriostatic Effect of NGAL

(A) Dashed lines indicate the growth of *E. coli* cultures, measured as OD₆₀₀, in M9 media at 37°C, plotted versus time; solid lines indicate growth in the presence of 5 μM NGAL.

(B) Endpoint saturations at 36 hr (OD₆₀₀) of *E. coli* cultures grown in M9 media at 37°C, supplemented with 5 μM NGAL and increasing concentrations of iron, are plotted.

NGAL:FeDHBx model likely reflect both the greater internal conformational freedom of FeDHBx relative to FeEnt and some slack in the position of the ligand in the calyx.

NGAL Is a Potent Bacteriostatic Agent

The specificity and high affinity of NGAL for bacterial catecholate-type ferric siderophores immediately suggests a function for this previously mysterious protein; NGAL is released by neutrophils at sites of infection and inflammation to sequester bacterial ferric siderophores, thus participating in the antibacterial iron-depletion strategy of the innate immune system. However, while other components of this system, such as lactoferrin, simply bind to and sequester free iron, NGAL is specific for iron already earmarked for bacterial use as ferric siderophore complexes. To test the hypothesis that NGAL directly interferes with siderophore-mediated iron uptake by bacteria, we investigated the effect of exogenous NGAL on the growth of bacteria under iron-limiting conditions. We had already noted that XL1-Blue *E. coli* expressing NGAL fail to grow in M9 minimal media unless supplemented with 10 μM iron. Although M9 is not normally supplemented with iron, the ubiquity of trace iron contamination in reagents and on glassware results in estimated residual iron concentrations of 0.1 μM (Klebba et al., 1982) to 2 μM (Roberts et al., 1963), which is sufficient for *E. coli* to grow to saturation, albeit at a much reduced rate (Figure 5A). However, the addition

of exogenous apo-NGAL, at a concentration of only 5 μM, resulted in a dramatic 20-fold inhibition of growth (Figure 5A). Adding iron just sufficient to saturate the NGAL present rescues growth (Figure 5B), demonstrating that NGAL does not have any antibacterial activity beyond iron sequestration.

For our functional hypothesis to be viable, the affinity of NGAL for ferric siderophores must be strong enough, the specificity broad enough, and the amount of NGAL in the body high enough to efficiently out-compete various bacterial ferric siderophore receptors. The K_d of FepA for FeEnt has been measured by fluorescence spectroscopy at 50 nM (Buchanan et al., 1999) and by filter binding at 0.2 nM (Newton et al., 1999), comparable to the affinity of NGAL for FeEnt. The calyx of NGAL, while specific for catecholate-type siderophores, utilizes extremely clever recognition machinery, not dependent upon highly shape-, size- and character-dependent van der Waals and hydrogen bond networks, that would instead likely allow a large range of catecholate-type siderophores to be bound tightly. NGAL is an acute phase protein, whose serum concentration can be used clinically to differentiate between bacterial and other types of infections (Xu and Venge, 2000). During inflammation, concentrations of NGAL can increase to levels, with concentrations approaching 20–30 nM in the serum, presumably adequate to bind all available iron as ferric siderophore complexes (Xu and Venge, 2000). This functional hypothesis also provides an explanation for why aerobactin is an *E. coli* virulence factor even though it has a lower affinity for iron than Ent (Wooldridge and Williams, 1993); NGAL would not interfere with aerobactin-mediated iron acquisition as it has no measurable affinity for hydroxamate-type siderophores.

Implications for Other Functions of NGAL

NGAL has been implicated as a participant in a variety of processes that appear unrelated to its ferric siderophore binding specificity: cell differentiation, tumorigenesis, and apoptosis (Devireddy et al., 2001; Kjeldsen et al., 2000). However, evidence for several uncharacterized mammalian siderophore-like growth factors (Fernandez-Pol, 1978) and iron transport factors (Craven et al., 1987; Hershko et al., 1978; Jones et al., 1980) has been reported over the years. In the companion paper to this report (Yang et al., 2002), 24p3 is reported to mediate kidney cell differentiation by binding to an iron-containing chromophore, participating in an alternate iron delivery pathway. We would predict, based on our current structural analysis of NGAL, that the 24p3 ligand is likely a catecholate-type siderophore and that the NGAL recognition machinery is flexible enough to include a range of such molecules, including putative mammalian ones. If mammals do synthesize catecholate-type siderophores that are used to shuttle iron or act as growth factors, NGAL may participate in a wide variety of cellular processes by playing a role in regulating their transport.

NGAL is also released from neutrophil granules in multiple forms: monomer, disulfide-linked homodimer, and a disulfide-linked heterodimer with gelatinase-B (matrix metalloproteinase-9 [MMP-9]) (Kjeldsen et al., 1993; Triebel et al., 1992). MMP-9 is a member of the

matrix metalloproteinase family of multidomain, zinc endopeptidases that proteolytically degrade components of the extracellular matrix (Brinckerhoff and Matrisian, 2002). It is difficult to reconcile NGAL's ligand specificity with a possible functional role for NGAL in a complex with MMP-9. Dimerization does not affect the structure of the protein (Goetz et al., 2000). A recent report suggests that NGAL can slightly accelerate the direct activation of promatrix metalloproteinases (Tschesche et al., 2001), but the proposed mechanism requires that NGAL bind a clearly incompatible ligand, the hydrophobic propeptide. If MMP-9 had some esterase activity against FeEnt-like compounds, bacterial ferric siderophores could be catalytically degraded, with NGAL providing substrate specificity—but there is no evidence to support this speculation.

Results from these and previous structural and functional studies of human NGAL show that the initially proposed specificity and function of this molecule were incorrect. We now show that NGAL binds bacterial catecholate-type ferric siderophores and acts as a potent bacteriostatic agent by sequestering iron. This immediately suggests that NGAL participates in the iron-depletion strategy of the innate immune system, complementing the function of lactoferrin in neutrophil granules. However, while lactoferrin chelates iron directly, NGAL is unique in that it is specific for iron reserved for bacterial use as a ferric siderophore complex. Classically, lipocalins derive their name from the ligand that they bind. Therefore, we propose that this protein be renamed "siderocalin."

Experimental Procedures

Iron and Ligand Binding Assays

Atomic absorption measurements were performed with a Perkin-Elmer (Shelton, CT) 405 graphite furnace atomic absorption spectrophotometer. Standard curves were generated by serial dilution of a reference iron standard (Acros Organics, Tournai, Belgium). Tryptophan fluorescence quenching was measured on a Hitachi (Tokyo, Japan) F-2500 fluorometer with 5 nm slit widths in Tris-buffered saline (pH = 7.4) plus 5 mM Tris(2-carboxyethyl)phosphine hydrochloride (Pierce, Rockford, IL) and 32 μ g/ml ubiquitin (Sigma, St. Louis, MO). Measurements were made at receptor concentrations of 22 nM for FeEnt and 120 nM for FeDHB. Fluorescence values were corrected for dilution upon addition of titrant, ligand-absorbance, ligand-fluorescence, and photo-induced quenching of receptor. Fluorescence data were analyzed by nonlinear regression analysis of fluorescence response versus free ligand concentration using a one-site binding model as implemented in DYNAFIT (Kuzmic, 1996). As negative controls, BSA was assayed for binding to FeEnt and hemin was assayed for affinity to NGAL. Neither exhibited saturation binding up to micromolar ligand concentrations (data not shown).

Crystallography

Holo-NGAL was expressed, purified, and crystallized from the XL1-Blue strain of *E. coli* (Stratagene) as described previously (Bundgaard et al., 1994; Goetz et al., 2000). Dehydration in a saturated ammonium sulfate/glycerol artificial mother liquor prior to cryopreservation and an engineered mutation (Cys87Ser) were used to improve crystal quality (trace disulfide-linked homodimers through Cys87 dramatically poison NGAL monomer crystals). Cu-K α diffraction data were collected from 20 to 3.4 Å resolution without merging Bijvoet pairs and with greater than 10-fold redundancy (99.5% complete; $R_{\text{sym}} = 12\%$; $I/\sigma_1 = 21$; 88.3% of possible anomalous pairs measured; mean anomalous difference = 15.8%). Diffraction data collected at ALS beamline 5.0.1 to 2.4 Å resolution were processed

using HKL2000 (Otwinowski and Minor, 1997; Table 1). The structure was phased by molecular replacement with EPMR (Kissinger et al., 1999), using a previously published structure of NGAL (PDB accession code 1QQS; Goetz et al., 2000) as the search model, and rebuilt using the XtalView software package (McRee, 1999). The ligand electron density was clearly distinct in the three calyces in the asymmetric unit and was not improved by noncrystallographic symmetry averaging, suggesting that ligand orientation confers some subtle effect on the structure of the protein, not apparent at this resolution, that breaks symmetry. A model for FeEnt was generated by energy minimization of the structure of vanadium Ent (Karpishin et al., 1993) after substituting in iron. Semiempirical calculations on FeEnt were carried out using the program SPARTAN (Wavefunction). Structures were refined with CNS (Brünger et al., 1998) by simulated annealing with torsional dynamics followed by positional and individual B factor refinement. Solvent molecules were added manually, and the structures were then refined in reMac5 (CCP4, 1994) using TLS parameter refinement (Winn et al., 2001) followed by positional and individual B factor refinement to $R_{\text{work}}/R_{\text{free}}$ values of 23.8%/27.9% for NGAL:FeEnt and 22.5%/27.1% for NGAL:FeDHBx (Table 1). Six separate TLS groups were refined, one for each protein molecule and each ligand molecule in the asymmetric unit. Care was taken to maintain the same R_{free} set throughout both refinements.

Acknowledgments

The authors would like to thank the following people for providing helpful suggestions and comments: Niels Anderson, Adrian Ferré D'Amaré, and Jefferson Foote. This work was supported by grants from the National Institutes of Health (AI42200) and the FHCR New Technology Development Fund to R.K.S.; D.H.G. was supported by a National Science Foundation Graduate Research Fellowship and a National Institutes of Health T32 training grant (GM0720).

Received: April 9, 2002

Revised: August 26, 2002

References

- Åkerstrom, B., Flower, D.R., and Salier, J.-P. (2000a). Lipocalins: unity in diversity. *Biochim. Biophys. Acta* 1482, 1–8.
- Åkerstrom, B., Flower, D.R., and Salier, J.-P., eds (2000b). Lipocalins 2000. *Biochim. Biophys. Acta* 1482, nos. 1–2.
- Berman, H.M., Westbrook, J., Feng, Z., Gilliland, G., Bhat, T.N., Weissig, H., Shindyalov, I.N., and Bourne, P.E. (2000). The Protein Data Bank. *Nucleic Acids Res.* 28, 235–242.
- Bjorkman, P.J., Saper, M.A., Samraoui, B., Bennett, W.S., Strominger, J.L., and Wiley, D.C. (1987). The foreign antigen binding site and T cell recognition regions of class I histocompatibility antigens. *Nature* 329, 512–518.
- Bratt, T., Ohlson, S., and Borregaard, N. (1999). Interactions between neutrophil gelatinase-associated lipocalin and natural lipophilic ligands. *Biochim. Biophys. Acta* 1472, 262–269.
- Braun, V., and Killmann, H. (1999). Bacterial solutions to the iron-supply problem. *Trends Biochem. Sci.* 24, 104–109.
- Brinckerhoff, C.E., and Matrisian, L.M. (2002). Matrix metalloproteinases: a tail of a frog that became a prince. *Nat. Rev. Mol. Cell Biol.* 3, 207–214.
- Brünger, A.T., Adams, P.D., Marius Clore, G., DeLano, W.L., Gros, P., Grosse-Kunstleve, R.W., Jiang, J.-S., Kuszewski, J., Nilges, M., Pannu, N.S., et al. (1998). Crystallography & NMR system: a new software suite for macromolecular structure determination. *Acta Crystallogr. D* 54, 905–921.
- Buchanan, S.K., Smith, B.S., Venkatramani, L., Xia, D., Esser, L., Palnitkar, M., Chakraborty, R., van der Helm, D., and Deisenhofer, J. (1999). Crystal structure of the outer membrane active transporter FepA from *Escherichia coli*. *Nat. Struct. Biol.* 6, 56–63.
- Bundgaard, J.R., Sengelov, H., Borregaard, N., and Kjeldsen, L. (1994). Molecular cloning and expression of a cDNA encoding NGAL:

- a lipocalin expressed in human neutrophils. *Biochem. Biophys. Res. Commun.* **202**, 1468–1475.
- Cao, Z., Qi, Z., Sprencel, C., Newton, S.M., and Klebba, P.E. (2000). Aromatic components of two ferric enterobactin binding sites in *Escherichia coli* FepA. *Mol. Microbiol.* **37**, 1306–1317.
- CCP4 (Collaborative Computational Project 4) (1994). The CCP4 suite: programs for protein crystallography. *Acta Crystallogr. D* **50**, 760–763.
- Chen, X., Schauder, S., Potier, N., Van Dorsselaer, A., Pelczar, I., Bassler, B.L., and Hughson, F. (2002). Structural identification of a bacterial quorum-sensing signal containing boron. *Nature* **415**, 545–549.
- Chu, S.T., Lin, H.J., and Chen, Y.H. (1997). Complex formation between a formyl peptide and 24p3 protein with a blocked N-terminus of pyroglutamate. *J. Pept. Res.* **49**, 582–585.
- Clarke, T.E., Braun, V., Winkelmann, G., Tari, L.W., and Vogel, H.J. (2002). X-ray crystallographic structures of the *Escherichia coli* periplasmic protein FhuD bound to hydroxamate-type siderophores and the antibiotic albomycin. *J. Biol. Chem.* **277**, 13966–13972.
- Coles, M., Diercks, T., Muehlenweg, B., Bartsch, S., Zolzer, V., Tschesche, H., and Kessler, H. (1999). The solution structure and dynamics of human neutrophil gelatinase-associated lipocalin. *J. Mol. Biol.* **289**, 139–157.
- Craven, C.M., Alexander, J., Eldridge, M., Kushner, J.P., Bernstein, S., and Kaplan, J. (1987). Tissue distribution and clearance kinetics of non-transferrin-bound iron in the hypotransferrinemic mouse: a rodent model for hemochromatosis. *Proc. Natl. Acad. Sci. USA* **84**, 3457–3461.
- Devireddy, L.R., Teodoro, J.G., Richard, F.A., and Green, M.R. (2001). Induction of apoptosis by a secreted lipocalin that is transcriptionally regulated by IL-3 deprivation. *Science* **293**, 829–834.
- Dougherty, D.A. (1996). Cation- π interactions in chemistry and biology: a new view of benzene, Phe, Tyr, and Trp. *Science* **271**, 163–168.
- Ellison, R.T. (1994). The effects of lactoferrin on gram-negative bacteria. *Adv. Exp. Med. Biol.* **357**, 71–90.
- Ferguson, A.D., Hofmann, E., Coulton, J.W., Diederichs, K., and Welte, W. (1998). Siderophore-mediated iron transport: crystal structure of FhuA with bound lipopolysaccharide. *Science* **282**, 2215–2220.
- Ferguson, A.D., Chakraborty, R., Smith, B.S., Esser, L., van der Helm, D., and Deisenhofer, J. (2002). Structural basis of gating by the outer membrane transporter FecA. *Science* **295**, 1715–1719.
- Fernandez-Pol, J.A. (1978). Isolation and characterization of a siderophore-like growth factor from mutants of SV40-transformed cells adapted to picolinic acid. *Cell* **14**, 489–499.
- Flower, D.R. (2000). Beyond the superfamily: the lipocalin receptors. *Biochim. Biophys. Acta* **1482**, 327–336.
- Flower, D.R., North, A.C., and Sansom, C.E. (2000). The lipocalin protein family: structural and sequence overview. *Biochim. Biophys. Acta* **1482**, 9–24.
- Gallivan, J.P., and Dougherty, D.A. (1999). Cation- π interactions in structural biology. *Proc. Natl. Acad. Sci. USA* **96**, 9459–9464.
- Gibson, F., and Magrath, D.I. (1969). The isolation and characterization of a hydroxamic acid (aerobactin) formed by *Aerobacter aerogenes* 62-1. *Biochim. Biophys. Acta* **192**, 175–184.
- Goetz, D.H., Willie, S.T., Armen, R.S., Bratt, T., Borregaard, N., and Strong, R.K. (2000). Ligand preference inferred from the structure of neutrophil gelatinase associated lipocalin. *Biochemistry* **39**, 1935–1941.
- Harrison, P.M., and Arosio, P. (1996). The ferritins: molecular properties, iron storage function and cellular regulation. *Biochim. Biophys. Acta* **1275**, 161–203.
- Hershko, C., Graham, G., Bates, G.W., and Rachmilewitz, E.A. (1978). Non-specific serum iron in thalassaemia: an abnormal serum iron fraction of potential toxicity. *Br. J. Haematol.* **40**, 255–263.
- Jones, R.L., Peterson, C.M., Grady, R.W., and Cerami, A. (1980). Low molecular weight iron-binding factor from mammalian tissue that potentiates bacterial growth. *J. Exp. Med.* **151**, 418–428.
- Karpishin, T.B., Dewey, T.M., and Raymond, K.N. (1993). The vanadium (IV) enterobactin complex: structural, spectroscopic, and electrochemical characterization. *J. Am. Chem. Soc.* **115**, 1842–1851.
- Kissinger, C.R., Gehlhaar, D.K., and Fogel, D.B. (1999). Rapid automated molecular replacement by evolutionary search. *Acta Crystallogr. D* **55**, 484–491.
- Kjeldsen, L., Johnsen, A.H., Sengeløv, H., and Borregaard, N. (1993). Isolation and primary structure of NGAL, a novel protein associated with human neutrophil gelatinase. *J. Biol. Chem.* **268**, 10425–10432.
- Kjeldsen, L., Cowland, J.B., and Borregaard, N. (2000). Human neutrophil gelatinase-associated lipocalin and homologous proteins in rat and mouse. *Biochim. Biophys. Acta* **1482**, 272–283.
- Klebba, P.E., McIntosh, M.A., and Neilands, J.B. (1982). Kinetics of biosynthesis of iron-regulated membrane proteins in *Escherichia coli*. *J. Bacteriol.* **149**, 880–888.
- Kuzmic, P. (1996). Program DYNFIT for the analysis of enzyme kinetic data: application to HIV proteinase. *Anal. Biochem.* **237**, 260–273.
- Loomis, L.D., and Raymond, K.N. (1991). Solution equilibria of enterobactin and metal-enterobactin complexes. *Inorg. Chem.* **30**, 906–911.
- McRee, D.E. (1999). XtalView/Xfit—A versatile program for manipulating atomic coordinates and electron density. *J. Struct. Biol.* **125**, 156–165.
- Neilands, J.B. (1981). Microbial iron compounds. *Annu. Rev. Biochem.* **50**, 715–731.
- Neilands, J.B. (1995). Siderophores: structure and function of microbial iron transport compounds. *J. Biol. Chem.* **270**, 26723–26726.
- Newton, S.M., Igo, J.D., Scott, D.C., and Klebba, P.E. (1999). Effect of loop deletions on the binding and transport of ferric enterobactin by FepA. *Mol. Microbiol.* **32**, 1153–1165.
- O'Brien, I.G., and Gibson, F. (1970). The structure of enterochelin and related 2,3-dihydroxy-N-benzoylserine conjugates from *Escherichia coli*. *Biochim. Biophys. Acta* **215**, 393–402.
- Otto, B.R., Verweij-van Vught, A.M., and MacLaren, D.M. (1992). Transferrins and heme-compounds as iron sources for pathogenic bacteria. *Crit. Rev. Microbiol.* **18**, 217–233.
- Otwinowski, Z., and Minor, W. (1997). Processing of X-ray diffraction data collected in oscillation mode. *Methods Enzymol.* **276**, 307–326.
- Pollack, J.R., and Neilands, J.B. (1970). Enterobactin, an iron transport compound from *Salmonella typhimurium*. *Biochem. Biophys. Res. Commun.* **38**, 989–992.
- Ponka, P., Beaumont, C., and Richardson, D.R. (1998). Function and regulation of transferrin and ferritin. *Semin. Hematol.* **35**, 35–54.
- Ratledge, C., and Dover, L.G. (2000). Iron metabolism in pathogenic bacteria. *Annu. Rev. Microbiol.* **54**, 881–941.
- Raymond, K.N., Müller, G., and Matzanke, B.F. (1984). Complexation of iron by siderophores. A review of their solution and structural chemistry and biological function. In *Topics in Current Chemistry*, F.L. Boschke, ed. (Berlin, Heidelberg: Springer-Verlag), pp. 50–102.
- Roberts, R.B., Abelson, P.H., Cowie, D.B., Bolton, E.T., and Britten, R.J. (1963). Studies of biosynthesis in *Escherichia coli*. In *Publication 607* (Washington: Carnegie Institute of Washington).
- Sengeløv, H., Boulay, F., Kjeldsen, L., and Borregaard, N. (1994). Subcellular localization and translocation of the receptor for N-formylmethionyl-leucyl-phenylalanine in human neutrophils. *Biochem. J.* **299**, 473–479.
- Triebel, S., Bläser, J., Reinke, H., and Tschesche, H. (1992). A 25 kDa α_2 -microglobulin-related protein is a component of the 125 kDa form of human gelatinase. *FEBS Lett.* **3**, 386–388.
- Tschesche, H., Zolzer, V., Triebel, S., and Bartsch, S. (2001). The human neutrophil lipocalin supports the allosteric activation of matrix metalloproteinases. *Eur. J. Biochem.* **268**, 1918–1928.
- Wallace, A.C., Laskowski, R.A., and Thornton, J.M. (1995). LIGPLOT: a program to generate schematic diagrams of protein-ligand interactions. *Protein Eng.* **8**, 127–134.
- Weichsel, A., Andersen, J.F., Champagne, D.E., Walker, F.A., and

- Montfort, W.R. (1998). Crystal structures of a nitric oxide transport protein from a blood-sucking insect. *Nat. Struct. Biol.* *5*, 304–309.
- Weinberg, E.D. (1984). Iron withholding: a defense against infection and neoplasia. *Physiol. Rev.* *64*, 65–102.
- Winn, M.D., Isupov, M.N., and Murshudov, G.N. (2001). Use of TLS parameters to model anisotropic displacements in macromolecular refinement. *Acta Crystallogr. D57*, 122–133.
- Wooldridge, K.G., and Williams, P.H. (1993). Iron uptake mechanisms of pathogenic bacteria. *FEMS Microbiol. Rev.* *12*, 325–348.
- Xu, S., and Venge, P. (2000). Lipocalins as biochemical markers of disease. *Biochim. Biophys. Acta* *1482*, 298–307.
- Yaffe, M.B. (2002). Phosphotyrosine-binding domains in signal transduction. *Nat. Rev. Mol. Cell Biol.* *3*, 177–186.
- Yang, J., Goetz, D., Li, J.-Y., Wang, W., Mori, K., Setlik, D., Du, T., Erdjument-Bromage, H., Tempst, P., Strong, R., and Barasch, J. (2002). Iron delivery pathway mediated by a lipocalin. *Mol. Cell* *10*, this issue, 1045–1056.

Accession Numbers

The coordinates of the NGAL:FeDHBx complex were deposited in the PDB under accession code 1L6M.